HAL
open science

Tailoring the textural properties of an activated carbon for enhancing its adsorption capacity towards diclofenac from aqueous solution

Adriana Moral-Rodríguez, Roberto Leyva-Ramos, Conchi Maria Concepcion Ovin Ania, Raul Ocampo-Pérez, Elizabeth Isaacs-Páez, Damarys Carrales-Alvarado, José Parra

To cite this version:

Adriana Moral-Rodríguez, Roberto Leyva-Ramos, Conchi Maria Concepcion Ovin Ania, Raul Ocampo-Pérez, Elizabeth Isaacs-Páez, et al.. Tailoring the textural properties of an activated carbon for enhancing its adsorption capacity towards diclofenac from aqueous solution. Environmental Science and Pollution Research, 2019, 26 (6), pp.6141-6152. 10.1007/s11356-018-3991-x . hal-02318749

HAL Id: hal-02318749

https://hal.science/hal-02318749v1

Submitted on 6 Nov 2020

HAL is a multi-disciplinary open access archive for the deposit and dissemination of scientific research documents, whether they are published or not. The documents may come from teaching and research institutions in France or abroad, or from public or private research centers.

L'archive ouverte pluridisciplinaire **HAL**, est destinée au dépôt et à la diffusion de documents scientifiques de niveau recherche, publiés ou non, émanant des établissements d'enseignement et de recherche français ou étrangers, des laboratoires publics ou privés.

Moral-Rodríguez AI, Leyva-Ramos R, Ania CO, Ocampo-Pérez R, Isaacs-Páez ED, Carrales-Alvarado DH, Parra JB, Tailoring the textural properties of an activatedcarbon for enhancing its adsorption capacity towards diclofenac from aqueous solution, Environ. Sci. Poll. Res. (2019) 1-12.

10.1007/s11356-018-3991-x

hal-02318749v1

TAILORING THE TEXTURAL PROPERTIES OF AN ACTIVATED CARBON FOR ENHANCING ITS ADSORPTION CAPACITY TOWARDS DICLOFENAC FROM AQUEOUS SOLUTION

Adriana I. Moral-Rodríguez[1], Roberto Leyva-Ramos[1]*, Conchi O. Ania[2], Raul Ocampo-Pérez[1], Elizabeth D. Isaacs-Páez[1], Damarys H. Carrales-Alvarado[1], Jose B. Parra[3]

[1] Centro de Investigación y Estudios de Posgrado, Facultad de Ciencias Químicas, UASLP, Av. Dr. Manuel Nava No. 6, San Luis Potosí, SLP 78210, México

*E-mail: rlr@uaslp.mx

[2]POR2E Group, CEMHTI (UPR 3079) CNRS, Univ. Orléans, Orléans, France

[3] Instituto Nacional del Carbón (INCAR, CSIC), Oviedo, España

ABSTRACT

A series of activated carbons (ACs) were prepared by modifying a commercial AC by physical activation using CO_2 during different activation times. The ACs were designated as F, F12, F24 and F40 corresponding to the activation times of 0, 12, 24 and 40 hours, respectively. The surface area, total pore volume, micropore volume and mean micropore width were determined for all the ACs. The textural properties of the modified ACs increased substantially with the activation time, and the capacity of the ACs for adsorbing diclofenac (DCF) was almost linearly dependent upon the surface area of the ACS. The maximum adsorption capacities of F, F12, F24 and F40 carbons towards diclofenac (DCF) from aqueous solution were 271, 522, 821 and 1033 mg/g, respectively. Hence, the adsorption capacities of ACs were considerably enhanced with the activation time, and F12, F24 and F40 carbons presented the highest adsorption capacities towards DCF reported in the technical literature. The F40 adsorption capacity was at least twice those of other carbon materials. The adsorption capacities decreased by raising the pH from 7 to 11 due to electrostatic repulsion between the ACs surface and anionic DCF in solution. The removal of DCF from a wastewater treatment plant (WWTP) effluent was effectively carried out by adsorption on F40. Hence, the capacity of ACs for adsorbing DCF can be optimized by tailoring the porous structure of ACs.

Keywords: Activated carbon; Adsorption; CO_2 activation; Diclofenac; Microporosity; Tailoring porosity

1. INTRODUCTION

Potential environmental and health problem due to water contamination caused by the presence of emerging pollutants is attracting attention to the society. Due to their worldwide consumption, pharmaceuticals and their metabolites represent an overwhelming portion of trace emerging contaminants detected in surface and drinking water, groundwater, and wastewaters (Houeto et al. 2012). Most commonly found pharmaceutical pollutants in effluents from wastewater treatment plants (WWTP) are antibiotics, antacids, antidepressants, analgesics, antipyretics, steroids, anti-inflammatory, β-blockers, tranquilizers and stimulants (Ternes 1998; Daughton and Ternes 1999; Rivera-Utrilla et al. 2009).

Nowadays, the non-steroidal anti-inflammatory drugs (NSAIDs) are extensively prescribed to cure many diseases and are the most widely used therapeutic group worldwide, which has led to its presence in different groundwater or surface water sources. Diclofenac (DCF) is an NSAID drug and is employed to decrease swelling and alleviate pain in pathologies such as rheumatoid arthritis. DCF has the highest critical toxicity within the NSAIDs, with a half maximal effective concentration (EC_{50}) less than 100 mg/L (Cleuvers 2003), and can be found in drinking water, groundwater, WWTP effluents and surface water supplies in several countries at concentration levels varying from ng/L to μg/L (Houeto et al. 2012).

The concentrations of pharmaceuticals in water resources seldom exceed the curative doses, but they are steadily released to the environment; so the concentrations remain almost constant, posing a critical hazzard to human health and environment (Richards et al. 2004). Most of them are hardly biodegradable and can be poorly eliminated and biodegraded by traditional biological treatment. Therefore, elimination of pharmaceuticals in WWTPs is a crucial topic of interest (Ternes et al. 2002; Clara et al. 2005; Watkinson et al. 2007; Kasprzyk-Hordern et al. 2009; Rúa-Gómez and Püttmann 2012), and there is a pressing need for improving current

treatment technologies. The efficiency of activated carbon adsorption technology as an end-of-pipe technology to upgrade existing WWTP to remove the emerging micropollutants has long been investigated (Carvalho et al. 2012, 2013).

The modification of activated carbons (ACs) for improving their capacities for adsorbing DCF has been studied in few works. For instance, Álvarez Torrellas et al. (2015) investigated the adsorption of diclofenac on chemical-activated carbon synthesized from peach stones. This AC was chemically modified with an HNO_3 solution to increase the acidic sites and was thermally modified to decrease the acidic groups. The pristine AC and the two modified ACs showed no adsorption capacity towards DCF for concentrations less than 20 mg/L, attributing this behavior to weak DCF-adsorbent interactions. In contrast, for concentrations above 20 mg/L, the uptake of DCF was continually increased by raising the concentration, and the capacity of pristine AC reached 200 mg/g for a concentration of DCF at equilibrium of 70 mg/L. Furthermore, the thermal modification of AC did not substantially influence the adsorption capacity, whereas the chemical modification reduced the adsorption capacity. Saucier et al. (2015) analyzed the pH dependence of the adsorption equilibrium and kinetics of DCF from aqueous solution on an AC produced by microwave-assisted chemical activation of coconut shell. The findings showed that the maximum uptake of DCF adsorbed was 63.47 mg/g at an optimal pH = 7. Álvarez et al. (2015) analyzed the adsorption of DCF on chemically modified carbon xerogels, attaining uptakes of 182.5 and 80 mg/g for the materials modified with urea and sulfuric acid, respectively. Lastly, the competitive adsorption of diclofenac in the presence of salicylic acid, acetylsalicylic acid and atenolol on three commercial ACs was examined by Rakić et al. (2015), with adsorption capacities ranging from 13.8 to 31 mg/g for all four pollutants.

In previous studies, it has been reported that the adsorption capacities of the ACs towards DCF varied from 13.8 to 347 mg/g; this is an essential issue for screening the adequate carbon adsorbent to be integrated into current water treatment technologies for removing DCF. The relation between the adsorption capacity of AC towards DCF and the surface chemistry of AC has been addressed; nevertheless, the role of the porous structure (surface area, pore diameter and pore volume) on the adsorption capacity has not been investigated completely. Consequently, the purpose of this work was to find out the relationship between the adsorption capacity of ACs towards DCF and their textural properties and to substantiate the optimal characteristics of an AC to maximize the capacity for adsorbing DCF. This work was aimed at preparing a series of nanoporous carbons by modifying a commercial AC by physical activation with CO_2 and varying the activation time, to develop further the porous structure and improve the adsorption capacity towards DCF from water solution. Additionally, the porous structure of ACs considerably affected the adsorption capacity, and the mechanism of DCF adsorption on AC was elucidated by conducting adsorption experiments at different pH.

2. EXPERIMENTAL METHODS

2.1 Materials

A commercial microporous carbon (sample F) obtained by steam activation of coconut shell (CPL, Carbon Link) was selected for this study. The particle size of carbon F ranged from 0.40 to 0.75 mm. Three nanoporous carbons having increasing burn-off degree were prepared by activating the carbon F under a CO_2 atmosphere (5 ºC/min up to 850 ºC in 100 mL/min N_2, afterward change to CO_2, 10 mL/min) (Gomis-Berenguer et al. 2016) during times of 12, 24 and 40 h. The carbon samples were designated as F12, F24 and F40, respectively.

2.2 Chemical and textural properties

The elemental composition of the ACs was quantified using elemental analyzers. The carbon, hydrogen and nitrogen were determined by a LECO CHNS-932 (ASTM D-5373), sulfur was quantified by a LECO S-144DR (ASTM D-4239) analyzer, and oxygen was evaluated with a LECO VTF-900 CHNS-932 microanalyzer. All the analysis have been done at least in triplicates with a standard deviation below 2 %. Besides, the pH at the point of zero charge (pH_{PZC}) was determined using a modification of the mass-titration method detailed elsewhere (Ania et al. 2007).

The porous structure of the samples was analyzed using the N_2 adsorption-desorption isotherms at 77 K. The measurements were performed in a high-resolution physisorption analyzer, Micromeritics, ASAP 2020, equipped with three pressure transducers and a molecular pump, allowing to improve the sensitiveness at low pressures. Strict conditions were programmed to ensure N_2 adsorption equilibrium so that the determination of each isotherm lasted on average between 90 and 120 h. Prior to the measurement, the outgassing of the carbon samples was carried out at 120 ºC overnight under vacuum. The surface area (S_{BET}) and total pore volume (V_P) were calculated from the N_2 adsorption isotherm. The micropore volume ($V_{Micro\text{-}NLDFT}$) and pore size distribution (PSD) were evaluated with the 2D-NLDFT-HS model, and considering that the surface of the carbon pores was heterogeneous (Jagiello and Olivier 2013b). The adsorption isotherms of CO_2 were measured in a volumetric analyzer (Tristar 3020, Micromeritics) at 273 K. The narrow microporosity (W_0) was evaluated by fitting the Dubinin-Radushkevich equation to the adsorption isotherm data of CO_2, and the Stoeckli and Ballerini (1991) equation was applied to estimate the average micropore width (L_0). The experimental isotherms were recorded in duplicates with an accuracy of ca. 2 %. The standard deviations

associated to the calculation of the textural parameters from the experimental data were below 2 %. Here, average data is presented.

Raman spectroscopy was performed by excitation with green laser light (532 nm) in the range between 800-3550 cm^{-1}. The spectra were acquired in a Jobin-Yvon Horiba HR800 spectrometer equipped with a Leica microscope. The acquisition time for each spectrum was 300 s; to guarantee a representative sampling, spectra were recorded in 4 different spots for each sample. The temperature programmed desorption experiments (TPD) were carried out in a chemisorption analyzer (Micromeritics, Autochem II) under and argon flow rate of 50 mL min^{-1}, at a heating rate of 10 ºC min^{-1} up to a final temperature of 1000 ºC. CO and CO_2 evolution was monitored by mass spectrometry (OmniStar 3000). Data was performed in duplicates (average date is presented), with an with an accuracy of ca. 5 %.

2.3 Adsorbate

Diclofenac sodium salt was provided by Sigma-Aldrich. The molecular structure and physicochemical properties of this anti-inflammatory are shown in Table 1. The density functional theory (DFT) was applied to obtain the molecular structure of DCF (Moral-Rodríguez et al. 2016).

2.4 Experimental adsorption equilibrium data

In this work, the DCF solutions were fixed by adding a given aliquot of a DCF stock solution into a volumetric flask (50 mL) and then, diluting using a solution having a constant ionic strength of 0.01 N and pH of 7, 9 or 11. The latter was made by mixing suitable volumes of 0.01 N HCl and NaOH solutions. The DCF solution was sampled, and the sample (10 mL) was

later analyzed to confirm the initial concentration of DCF, which varied from 400 to 2000 mg/L. The concentration of DCF in water samples was quantified by a UV-Visible spectrophotometric method, and the absorbance of DCF in an aqueous solution was measured in a spectrophotometer, Shimadzu UV 2600, at a wavelength of 276 nm.

An experimental batch adsorber was used to obtain the adsorption equilibrium data of DCF on ACs. A specific mass of the AC (25 mg) and volume of DCF solution (40 mL) were added in a centrifugal vial (50 mL), which was the batch adsorber. Thereupon, the vial was partially immersed in a thermostatic bath. The adsorbent and the solution were allowed to equilibrate during 7 days. Once the experiments reached equilibrium, an aliquot (10 mL) was sampled, and the concentration of DCF at equilibrium was quantified by the method explained previously. The pH of the solution in the adsorber was determined periodically during the adsorption experiment, and was maintained constant at a given value by the addition of few drops of 0.01 M HCl y NaOH solutions. Changes in the adsorber solution volume due to pH adjustment were considered negligible because they were less than 1.0 %.

The uptake of DCF adsorbed on the ACs was computed by carrying out a mass balance, which is represented by the subsequent mathematical expression:

$$q = \frac{V(C_0 - C_e)}{m} \qquad \textbf{(1)}$$

Where q is the mass of DCF adsorbed on AC, mg/g; C_0 is the initial concentration of DCF, mg/L; C_e is the concentrattion of DCF at equilibrium, mg/L; m is the mass of AC, g; and V is the solution volume in the adsorber, L. The error associated to the determination of DCF was found to be lower than 1.5 %, assuring that the deviations in the estimation of the uptake are lower than 4 % in all cases.

The adsorption of DCF in the effluent from a WWTP was carried out to study the actual application of the F and F40 for removing DCF. The adsorption of DFC was determined by contacting the ACs with a solution prepared by spiking DCF in a sample of an effluent from a WWTP situated in the city of San Luis Potosí, SLP, Mexico. The initial and equilibrium concentrations of DCF, TC and TOC in the solution were quantified as explained earlier. The pH of the wastewater solution was not adjusted nor maintained constant during the adsorption of DCF.

2.5 Quantification of Total Organic Carbon

The total carbon (TC), the inorganic carbon (IC) and the total organic carbon (TOC) of water samples were determined in a TOC analyzer, Shimadzu TOC-L, equipped with an autosampler ASI-L. The TC was measured by injecting a water sample into the reaction chamber packed with an oxidizing catalyst, and the oxidation of TC (organic and inorganic carbon) generated CO_2 at T = 680 °C. Then, the IC was evaluated by injecting the sample into the chamber containing phosphoric acid. Under acidic conditions, the organic carbon was not oxidized, and the IC was converted into CO_2. The difference between the TC and IC resulted in the TOC. The experimental error in TOC analysis was lower than 5% (average data is presented).

3. RESULTS AND DISCUSSION

3.1 Variation of the ACs properties with the activation time

The primary purpose of this work was to ascertain the optimal porous properties of ACs for removing DCF from aqueous solution. The pristine AC was modified to enhance its porosity

and enable access to the internal surface area, to maximize its adsorption capacity towards DCF. The pristine AC was subjected to physical activation with CO_2 during varying activation times.

The adsorption isotherms of N_2 of the four ACs at 77 K are depicted in Fig. 1(a), and based upon IUPAC classification (Rouquerol et al. 2014), the shapes of the adsorption isotherm were representative of type Ia for F, F12 and F24, that is typical of greatly microporous ACs with a distribution of micropore sizes mainly below 1 nm. In contrast, sample F40 showed an isotherm of type Ib featuring a wide knee at low relative pressures, typical of materials having larger micropores and narrow mesopores. The opening of the isotherm knee and the total volume of N_2 adsorbed increased gradually with the activation time, which was attributed to the widening of pore size and the enlargement of the micropore volume during the activation.

The principal textural properties of the ACs are listed in Table 2, and all these properties increased with the activation time. It can be noted that the S_{BET} of F40 carbon increased almost 2.3 times compared to the S_{BET} of F carbon. Additionally, the values of V_P, W_0, V_{Micro} and L_0 for F carbon were more than doubled after 40 hours of activation.

The N_2 adsorption-desorption isotherm was interpreted with the 2D-NLDFT-HS model (Jagiello and Olivier 2013a) to evaluate the PSD of all the ACs (See Fig. 1(b)). This figure corroborates the formation and widening of the large micropores (0.7 nm > d_p > 2 nm) for F12, F24 and F40 carbons as the activation time progressed. Notably, the increase in the micropores in the range of 1-2 nm was more pronounced for F40 carbon. The micropore volume of F40 carbon (V_{Micro}, $W_{o,\ N2}$ and $W_{o,\ CO2}$) was almost twice that of F carbon (See Table 2), confirming the development of microporosity along the activation time.

Additionally, the adsorption isotherms of CO_2 were determined to evaluate the narrow microporosity of the ACs (Garrido et al. 1987; Contreras et al. 2010) at 273 K, and are graphed

in Fig. 2, showing the development of micropores as the activation time increased. At low relative pressures less than 0.010, the volume of CO_2 adsorbed on F12 and F40 carbons was lower than that on the pristine carbon, confirming the enlargement of the narrow micropores with the activation time. Moreover, the volume of CO_2 adsorbed on F40 was less than that of F24, indicating that the narrow microporosity decreased at the expense of increasing the total micropore volume. The adsorption isotherm of CO_2 on the pristine carbon intersects those on the modified carbons, demonstrating that the activation favors the enlargement of the micropores. The changes in the porosity did not have an impact in the structure of the series of carbons, as inferred from Raman spectroscopy (Figure Sx in the Supporting File).

Regarding the chemical composition, the successive activation of the carbons barely modified their composition, as can be inferred from the values of the elemental analysis listed in Table 3. The carbon content in all the ACs is higher than 95 wt.%, whereas that of oxygen is less than 4 wt.%. The oxygen content increases slightly with the activation time; however, the low oxygen contents reveal that all ACs have a minimal quantity of O-surface groups. This was quantification of the CO and CO_2-evolving groups determined by TPD-MS (Table 3), and the evolution of the pH of the point of zero charge upon activatin, rendering carbons with a slightly more basic character.

In sum, the characterization results confirmed that the activation time with CO_2 only provoked changes in the porosity of thecarbons, with no signification influence on the structure and chemical nature of the carbon surface.

3.2 Diclofenac adsorption isotherms

The experimental adsorption equilibrium data of DCF on the ACs were interpreted by the Radke-Prausnitz (R-P) isotherm model. This isotherm model was selected because, as argued later, the isotherm shape of F carbon was different from the isotherm shapes of the modified carbons. Besides, the R-P isotherm combines the characteristics of the Freundlich and Langmuir isotherms. The R-P model can be expressed by the subsequent equation:

$$q = \frac{aC}{1 + bC^{\beta}} \qquad \textbf{(2)}$$

where a ($L\ g^{-1}$), b ($L^{\beta}\ mg^{-\beta}$) and β are the isotherm constants.

The R-P isotherm model was fitted to the experimental data, and the isotherm constants were computed by a regression method employing the nonlinear algorithm of Rosenbrock-Newton. The isotherm parameters and the values of the average percentage deviations (%D) are given in Table 4. The subsequent equation was applied to estimate %D:

$$\%D = \left(\frac{1}{N} \sum_{i=1}^{N} \left| \frac{q_{exp} - q_{pred}}{q_{exp}} \right| \right) \times 100\ \% \qquad \textbf{(3)}$$

Where N is the number of experimental data; q_{exp} is the experimental uptake of DCF adsorbed, mg/g; and q_{pred} is the uptake of DCF adsorbed estimated by the R-P isotherm model, mg/g. The R-P model fitted the experimental data satisfactorily because the %D varied from 0.18 to 9.34 %.

The adsorption isotherms of DCF on F, F12, F24 and F40 carbons at 25 °C and pH of 7 are depicted in Fig. 3, and significant differences can be noticed on both the isotherm shapes and adsorption capacities of four carbons. The adsorption isotherms on all modified carbons show a Langmuir-type isotherm with a steep rise at low concentrations of DCF and leveling off at equilibrium concentrations of DCF greater than 1200 mg/L. This behavior is characteristic of adsorbents having energetically homogeneous surfaces. For carbon F, the trend of adsorption equilibrium data of DCF was different, and the uptake of DCF increases by raising the

concentration of DCF and does not level off or reach a plateau even at concentrations of DCF at equilibrium as high as 1500 mg/g. This behavior is commonly observed in materials showing energetically heterogeneous surface. Thus, the surfaces of the modified carbons are more energetically homogenous than the surface of the pristine carbon.

3.3 Influence of the activation time on the AC capacity for adsorbing DCF

As illustrated in Fig. 3, the capacity of the ACs for adsorbing DCF from aqueous solution was considerably affected by the activation time and the decreasing order of the adsorption capacities was as follows: F40 > F24 > F12 > F. As shown in this figure, the maximum experimental adsorption capacities of F40, F24, F12, and F carbons were 1033, 821, 522 and 271 mg/g, correspondingly. A comparison of the adsorption capacities of all ACs can be performed by estimating the uptake of DCF adsorbed at an equilibrium concentration of DCF of 1200 mg/L, and these values are referred to as Q_{1200}. The concentration of 1200 mg/L was chosen as the value closest to the maximum uptake where experimental data is available for all the carbons. The values of Q_{1200} were predicted from the R-P adsorption models and are listed in Table 4. Analyzing the vales of Q_{1200}, the adsorption capacities of F12, F24, and F40 carbons were enhanced 2.15, 2.85 and 3.85 times as a result of the activation time. This enhancement can be primarily attributed to the modification of the textural properties that favored the adsorption capacity by increasing the surface area and widening of the pore size. Comparable findings have been previously presented throughout the literature for the adsorption of organic compounds on ACs (Mestre et al. 2009; Nowicki et al. 2015).

The relationship between the adsorption capacity of ACs towards DCF and the textural properties was further studied by plotting the maximum adsorption capacity (Q_{1200}) versus the

surface area, S_{BET}, and the results are shown in Fig. 4(a). As expected, Q_{1200} increased almost linearly concerning S_{BET}, and this tendency can be due to that the capacity of ACs for adsorbing organic compounds is highly affected by the magnitude of S_{BET}. The effect of S_{BET} on Q_{1200} can be incorporated by recalculating the uptake per unit of surface area using the following equation:

$$U_{Norm} = \frac{Q_{1200}}{S_{BET}} \quad \textbf{(4)}$$

where, U_{Norm} is the normalized uptake of DCF per unit of surface area, mg/m^2.

The dependence of U_{Norm} on the pore volumes (V_P and V_{Micro}) and average micropore width (L_0) is also illustrated in Fig. 4(b-d), and as seen in these figures, U_{Norm} varied similarly concerning the textural properties V_p, V_{Micro} and L_0. Furthermore, it can be observed that U_{Norm} increases slightly and almost linearly for the F, F12 and F24 carbons, U_{Norm} reached a maximum value for F24 carbon, and then U_{Norm} was reduced for F40 carbon. It is essential to mention that the value of U_{Norm} increased with the activation time for the ACs with average micropore width ranging between 1.4 and 1.6 nm, but U_{Norm} for F40 carbon dropped when the micropores are widened over this range. This trend reveals that the longer activation times do not favor the adsorption capacity and the critical role of the pore dimensions on the adsorption capacity.

Although Q_{1200} raised as a result of increasing the pore volume and surface area of ACs, the decrease in U_{Norm} for F40 carbon demonstrated that the porosity of F24 carbon was more effectively utilized than that of F40 carbon (see Fig. 4(b-d)). For application purposes, the F24 carbon represents the most viable option, taking into account the costs associated with the additional activation time required for synthesizing F40 carbon. This result indicates that F24 carbon is the material whose activation conditions optimized the textural properties for removing DCF efficiently from water solutions.

3.4 Dependence of the adsorption capacity on the solution pH

The solution pH can dramatically influence the capacity of ACs for adsorbing ionizable compounds, as it may affect the charge of the AC surface and the species of DCF existing in aqueous solution. The effect of the solution pH on the capacity of F40 carbon for adsorbing DCF was examined by determining the adsorption isotherms at pH of 7, 9 and 11. Experimental adsorption equilibrium data was not procured at pH below 6 because of the low solubility of DCF. A white solid was formed in a DCF solution when the solution pH was reduced below 6. Carbon F40 was chosen because it presented the largest uptake and the highest concentration of functional groups containing oxygen (Table 2). The corresponding adsorption isotherms are depicted in Fig. 5, showing a remarkable reduction in the uptake of DCF adsorbed by raising the solution pH from 7 to 11.

In accordance to the speciation diagram of DCF in aqueous solution (Fig. 6), the DCF can predominantly be as a non-ionizable molecule at pH < 2, and as an anionic or deprotonated species at pH > 6. In this work, the anionic molecule (DCF^-) was the only species present because all the experiments were conducted at pH > 6. Furthermore, the solution pH also affected the surface charge of the nanoporous ACs. The pH_{PZC} of the ACs varied within the range 8.5-9.2 (Table 2), so that the surface of the ACs had a positive charge at pH = 7, and negative at pH = 11. At pH = 7, the DCF^- species were attracted to the surface of ACs whereas there was repulsion between the DCF^- species and the surface of ACs at pH = 11. Thus, the adsorption capacity was lessened by increasing the solution pH. This result can be explained recalling that the adsorption capacity was favored by the electrostatic attraction at pH = 7 and was diminished by the electrostatic repulsion at pH = 11.

The reduction of the adsorption capacity for F40 caused by increasing the solution pH was evaluated by comparing Q_{1200} estimated at pH of 7, 9 and 11. The values of Q_{1200} for F40 carbon at pH 7, 9 and 11 are given in Table 4. Thus, the adsorption capacity of F40 was reduced approximately 1.37 and 1.78 times by increasing the solution pH from 7 to 9, and from 7 to 11, correspondingly. The magnitude of this decrease in adsorption capacity indicates that the electrostatic interactions contributed significantly to the adsorption mechanism of the anionic species of DCF.

3.5 Adsorption mechanism of DCF

It is very well documented that the aromatic compounds can be predominantly adsorbed on ACs by the dispersive interactions due to π-electrons of the aromatic ring of the organic compound and π-electrons of the graphene layers of the ACs (Coughlin and Ezra 1968). The π-π dispersive interactions are highly affected by the surface area and accessibility to surface area. Indeed, the activation of a carbon adsorbent increases the number of graphene layers available, while the widening of the micropore width ensures the accessibility to the surface area. The adsorption capacity of the ACs raised almost linearly by increasing the surface area, corroborating that the dispersive interactions significantly influenced the adsorption of DCF on ACs. Furthermore, the adsorption capacity of ACs may be favored or disfavored by the electrostatic interactions between the ACs surface charge and the DCF species present in water solution.

3.6 Comparison of adsorption capacities of carbon materials

The maximum adsorption capacities of F carbon series were compared to those of other carbonaceous adsorbents published throughout the literature, and the maximum capacities for adsorbing DCF are listed in Table 5. The comparison was only among carbon-based materials because these materials usually exhibit high adsorption capacities towards organic compounds from water solution. Many different types of carbon materials have been investigated for adsorbing DCF from aqueous solutions, among these materials are activated carbons and biochars from various precursors, graphene oxide, expanded graphite, xerogels and carbon nanotubes. As shown in Table 5, the adsorption capacities of herein modified carbons are larger than those for the other carbon-based materials reported in previous works. The adsorption capacity of F40 was twice those of a porous carbon synthesized by pyrolyzing of metal azolate framework-6 (MAF-6) (An et al. 2018), and graphene oxide Nam et al. (2015), and about three times that of an AC commercially known as F400 (Moral-Rodríguez et al. 2016). Thus, the F40 presented the highest capacity of all carbonaceous adsorbents reported throughout the literature so far.

The capacity of each AC was normalized by dividing it by its surface area, and the adsorption capacity per unit of surface area was also listed in Table 5. Again, the DCF adsorption capacities of F40, F24 and F12 per unit surface area outperformed those of other carbon materials reported in the literature. The normalized adsorption capacity of F24 was nearly 4 times that of MAF-6 carbon, and the normalized capacity of the commercial activated carbon F400 is slightly greater than that of carbon F. The adsorption capacity per unit surface area is highly dependent on the accessibility of DCF to the pores of the carbon materials. Greater normalized adsorption capacity means that the surface area of the adsorbent is more efficiently

used for adsorbing DCF. All the above findings show the paramount importance of tailoring the textural properties of the ACs for achieving an elevated uptake of DCF.

3.7 Removal of DCF from a sample of water effluent from a WWTP

The effect of the water matrix upon the capacity of the F and F40 carbons for adsorbing DCF was investigated by removing DCF from the effluent of a WWTP. The solution of DCF was prepared by spiking DCF in an effluent sample from a municipal WWTP, and the dosage of ACs was 1.25 g/L. The adsorption isotherms of DCF on the F and F40 carbons from the water sample of WWTP are depicted in Fig. 7. Besides, the Radke-Prausnitz isotherm modeled the adsorption equilibrium data of DCF from WWTP, and the values of %D and adsorption isotherm constants are included in Table 4.

As seen in Fig. 7, the capacities of F and F40 carbons for adsorbing DCF were reduced in the WWTP solution. The values of Q_{1200} for carbons F and F40 in the WWTP solution were estimated to be 129 and 679 mg/g, respectively (See Table 4), and comparing these results with those in the buffer solution at pH = 7, it can be noticed that the Q_{1200} of the F and F40 carbons were decreased 47.1 % and 27.8 %. This result was somewhat expected because the effluent of a WWTP contains several inorganic and organic compounds, which may compete with the DCF for the adsorption sites of F and F40 ACs. The higher decrease of the adsorption capacity of carbon F than that of F40 could be attributed the narrow porosity of carbon F, which would be clogged up more easily upon adsorption of other organic pollutants present in the WWTP.

The application of the F40 carbon in WWTP was studied by evaluating the removal of DCF, TC and OC by adsorption on F40 from the WWTP effluent sample for a DCF initial concentration of 674 mg/L. The concentrations of DCF, TC and OC in the WWTP samples are

given in Table 6, and the progress of other relevant water quality parameters (IC, pH, conductivity and others) were also determined but were not reported in this work because their variation during adsorption was not crucial for removing of DCF. The percentage removal of DCF, TOC and OC were 77.7, 79.8 and 88.1 %, correspondingly. Consequently, the removal of DCF from WWTP solution can be effectively performed by adsorption on F40 carbon.

4. CONCLUSIONS

The adsorption capacity of ACs towards DCF from aqueous solutions was significantly affected by the porous structure of the ACs. The textural properties of the ACs were considerably modified by physical activation with CO_2 during different times, and the surface area was raised, and the micropores were widened by increasing the activation time. The surface chemistry of the ACs was slightly modified by the physical activation with CO_2, so differences in the adsorption capacity were mainly attributed to change in the textural properties of the ACs.

The adsorption capacities of ACs were enhanced by increasing the activation time. The adsorption capacities of the ACs increased almost linearly with the S_{BET}, V_P, W_0 and L_0. Furthermore, the maximum adsorption capacities of the modified ACs were well above those reported in the literature. The F24 carbon presented the highest normalized uptake of DCF adsorbed so that the F24 carbon had the optimal textural characteristics to remove DFC efficiently from aqueous solution. Consequently, the capacity of AC for adsorbing DCF can be maximized by the proper modification of its textural properties.

The capacity of ACs for adsorbing emerging pollutants can be considerably enhanced by tailoring the textural properties of the ACs. The concentration of DCF in a WWTP effluent was

effectively reduced by adsorption on F40, attaining a percentage removal of 77.7 % of this pollutant, along with a large removal of TOC and TC.

ACKNOWLEDGMENTS

This work was supported by Consejo Nacional de Ciencia y Tecnologia, CONACyT, Mexico (grants numbers INFR-2012-01-188381 and CB-2012-02-182779). COA and JBP thank the support of the Spanish MINECO (grant number CTM2014/56770-R).

REFERENCES

Álvarez S, Ribeiro RS, Gomes HT, Sotelo JL, García J (2015) Synthesis of carbon xerogels and their application in adsorption studies of caffeine and diclofenac as emerging contaminants. Chem Eng Res Des 95:229–238.

Álvarez Torrellas S, García Lovera R, Escalona N, Sepúlveda C, Sotelo JL, García J (2015) Chemical-activated carbons from peach stones for the adsorption of emerging contaminants in aqueous solutions. Chem Eng J 279:788–798.

Álvarez Torrellas S, Muñoz M, Zazo JA, Casas JA, García J (2016) Synthesis of high surface area carbon adsorbents prepared from pine sawdust-Onopordum acanthium L. for nonsteroidal anti-inflammatory drugs adsorption. J Environ Manage 183:294–305.

An HJ, Bhadra BN, Khan NA, Jhung SH (2018) Adsorptive removal of wide range of pharmaceutical and personal care products from water by using metal azolate framework-6 derived porous carbon. Chem Eng J 343:447–454.

Ania CO, Cabal B, Parra JB, Pis JJ (2007) Importance of the hydrophobic character of activated carbons on the removal of naphthalene from the aqueous phase. Ads Sci Technol 25: 155−168.

Carvalho AP, Mestre AS, Haro M, Ania CO (2012) Advanced methods for the removal of acetaminophen from water in A. Javaherian, P: Latifpour (Eds) Acetaminophen, Properties, Clinical Uses and Adverse Effects, Nova Science Publishers Inc, New York, pp 57−105.

Carvalho AP, Mestre AS, Andrade M, Ania CO (2013) Ibuprofen in the aquatic environment: Occurrence, ecotoxicity and water remediation technologies, in: W.C. Carter, B.R. Brown (Eds) Ibuprofen: Clinical Pharmacology Medical Uses and Adverse Effects, Nova Science Publishers Inc, New York, pp 1−60.

Clara M, Strenn B, Gans O, Martinez E, Kreuzinger N, Kroiss H (2005) Removal of selected pharmaceuticals, fragrances and endocrine disrupting compounds in a membrane bioreactor and conventional wastewater treatment plants. Water Res 39:4797–807.

Cleuvers M (2003) Aquatic ecotoxicity of pharmaceuticals including the assessment of combination effects. Toxicol Lett 142:185−194.

Contreras MS, Páez CA, Zubizarreta L, Léonard A, Blacher S, Olivera-Fuentes CG, Arenillas A, Pirard JP, Job N (2010) A comparison of physical activation of carbon xerogels with carbon dioxide with chemical activation using hydroxides. Carbon 48:3157–3168.

Coughlin RW, Ezra FS (1968) Role of surface acidity in the adsorption of organic pollutants on the surface of carbon. Environ Sci Technol 2:291–297.

Daughton CG, Ternes TA (1999) Pharmaceuticals and personal care products in the environment: Agents of subtle change?. Environ Health Perspect 107:907−938.

De Franco MAE, de Carvalho CB, Bonetto MM, de Pelegrini Soares R, Féris LA (2018) Diclofenac removal from water by adsorption using activated carbon in batch mode and fixed-bed column: Isotherms, thermodynamic study and breakthrough curves modeling. J Clean Prod 181:145–154.

Garrido J, Linares- Solano A, Martin- Martinez JM, Molina-Sabio M, Rodriguez- Reinoso F, Torregrosa R (1987) Use of nitrogen vs. carbon dioxide in the characterization of activated carbons. Langmuir 3:76–81.

Gomis-Berenguer A, Iniesta J, Moro A, Maurino V, Lima JC, Ania CO (2016) Boosting visible light conversion in the confined pore space of nanoporous carbons, Carbon 96:98-104.

Houeto P, Carton A, Guerbet M, Mauclaire AC, Gatignol C, Lechat P, Masset D (2012) Assessment of the health risks related to the presence of drug residues in water for human consumption: Application to carbamazepine. Regul Toxicol Pharm 62:41−48.

Jagiello J, Olivier JP (2013a) Carbon slit pore model incorporating surface energetical heterogeneity and geometrical corrugation. Adsorption 19:777–783.

Jagiello J, Olivier JP (2013b) 2D-NLDFT adsorption models for carbon slit-shaped pores with surface energetical heterogeneity and geometrical corrugation. Carbon 55:70–80.

Jodeh S, Abdelwahab F, Jaradat N, Warad I, Jodeh W (2015) Adsorption of diclofenac from aqueous solution using Cyclamen persicum tubers based activated carbon (CTAC). J Association of Arab Univ for Basic and App Sci 20:32–38.

Jung C, Boateng LK, Flora JRV, Oh J, Braswell MC, Son A, Yoon Y (2015) Competitive adsorption of selected non-steroidal anti-inflammatory drugs on activated biochars: Experimental and molecular modeling study. Chem Eng J 264:1–9.

Kasprzyk-Hordern B, Dinsdale RM, Guwy AJ (2009) The removal of pharmaceuticals, personal care products, endocrine disruptors and illicit drugs during wastewater treatment and its impact on the quality of receiving waters. Water Res 43:363–380.

Malhotra M, Suresh S, Garg A (2018) Tea waste derived activated carbon for the adsorption of sodium diclofenac from wastewater: adsorbent characteristics, adsorption isotherms, kinetics, and thermodynamics. Environ Sci Pollut Res. https://doi.org/10.1007/s11356-018-3148-y.

Mestre AS, Pires J, Nogueira JMF, Parra JB, Carvalho AP, Ania CO (2009) Waste-derived activated carbons for removal of ibuprofen from solution: Role of surface chemistry and pore structure. Bioresource Technol 100:1720–1726.

Moral-Rodríguez AI, Leyva-Ramos R, Ocampo-Pérez R, Mendoza-Barron J, Serratos-Alvarez IN, Salazar-Rabago JJ (2016) Removal of ronidazole and sulfamethoxazole from water solutions by adsorption on granular activated carbon: equilibrium and intraparticle diffusion mechanisms. Adsorption 22:89–103.

Nam SWD, Choi J, Kim SK, Her N, Zoh KD (2014) Adsorption characteristics of selected hydrophilic and hydrophobic micropollutants in water using activated carbon. J Hazard Mater 270:144–152.

Nam SW, Jung C, Li H, Yu M, Flora JRV, Boateng LK, Her N, Zoh K-D, Yoon Y (2015) Adsorption characteristics of diclofenac and sulfamethoxazole to graphene oxide in aqueous solution. Chemosphere 136:20–26.

Nowicki P, Kazmierczak J, Pietrzak R (2015) Comparison of physicochemical and sorption properties of activated carbons prepared by physical and chemical activation of cherry stones. Powder Technol 269:312–319.

Rakić V, Rac V, Krmar M, Otman O, Auroux A (2015) The adsorption of pharmaceutically active compounds from aqueous solutions onto activated carbons. J Hazard Mater 282:141–149.

Rouquerol F, Rouquerol J, Sing KSW, Llewellyn P, Maurin G (2014) Adsorption by powders and porous solids: Principles, methodology and applications. Academic Press, London.

Saucier C, Adebayo MA, Lima EC, Cataluña R, Thue PS, Prola LDT, Puchana-Rosero MJ, Machado FM, Pavan FA, Dotto GL (2015) Microwave-assisted activated carbon from cocoa shell as adsorbent for removal of sodium diclofenac and nimesulide from aqueous effluents. J Hazard Mater 289:18–27.

Stoeckli F, Ballerini L (1991) Evolution of microporosity during activation of carbon. Fuel 70:557–559.

Sotelo JL, Ovejero G, Rodríguez A, Álvarez S, Galán J, García J (2014) Competitive adsorption studies of caffeine and diclofenac aqueous solutions by activated carbon. Chem Eng J 240:443–453.

Richards SM, Wilson CJ, Johnson DJ, Castle DM, Lam M, Mabury SA, Sibley PK, Solomon KR (2004) Effects of pharmaceutical mixtures in aquatic microcosms. Environ Toxicol Chem 23:1035–1042.

Rivera-Utrilla J, Prados-Joya G, Sánchez- Polo M, Ferro-García MA, Bautista-Toledo I (2009) Removal of nitroimidazole antibiotics from aqueous solution by adsorption/bioadsorption on activated carbon. J Hazard Mater 170:298−305.

Rúa-Gómez PC, Püttmann W (2012) Occurrence and removal of lidocaine, tramadol, venlafaxine, and their metabolites in German wastewater treatment plants. Environ Sci Pollut Res 19: 689–99.

Ternes TA (1998) Occurrence of drugs in German sewage treatment plants and rivers. Water Res 32:3245−3260.

Ternes TA, Meisenheimer M, McDowell D, Sacher F, Brauch H-J, Haist-Gulde B, Preuss G, Wilme U, Zulei-Seibert N (2002) Removal of pharmaceuticals during drinking water treatment. Environ Sci Technol 36:3855–3863.

Vedenyapina MD, Borisova DA, Simakova AP, Proshina LP, Vedenyapin AA (2013) Adsorption of diclofenac sodium from aqueous solutions on expanded graphite. Solid Fuel Chem 47:59–63.

Watkinson JA, Murby EJ, Costanzo SD (2007) Removal of antibiotics in conventional and advanced wastewater treatment: Implications for environmental discharge and wastewater recycling. Water Res 41:4164–4176.

Wei H, Deng S, Huang Q, Nie Y, Wang B, Huang J, Yu G (2013) Regenerable granular carbon nanotubes/alumina hybrid adsorbents for diclofenac sodium and carbamazepine removal from aqueous solution. Water Res 47:4139–4147.

Table 1. Molecular structure and physicochemical properties of DCF.

Drug	Molecular structure	Molecular weight (g/mol)	Size X,Y,Z (Å)	Log K_{ow}[a]	pKa
Diclofenac sodium $C_{14}H_{10}C_{l2}NNaO_2$ (DCF)	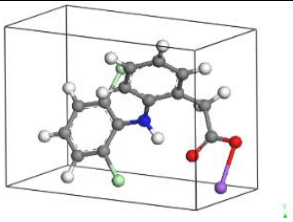	318.13	X: 0.960 Y: 0.708 Z: 0.472	3.91[b]	4.15

[a] Octanol-water partition coefficient.
[b] Nam et al. (2014).

Table 2. Textural properties of the F, F12, F24 and F40 carbons.

Activated Carbon	S_{BET} (m^2/g)	V_P[a] (cm^3/g)	V_{Meso}[b,c] (cm^3/g)	V_{Micro}[b] (cm^3/g)	$W_{o,\ N2}$[c] (cm^3/g)	L_0[d] (nm)	$W_{o,\ CO2}$[c] (cm^3/g)
F	799	0.35	0.03	0.31	0.37	0.91	0.25
F12	1146	0.50	0.04	0.45	0.55	1.37	0.33
F24	1279	0.58	0.06	0.50	0.64	1.56	0.37
F40	1801	0.86	0.15	0.66	0.80	2.00	0.36

[a] Total pore volume determined at $P/P^0 \approx 0.99$.

[b] Calculated from 2D-NLDFT-HS model (Jagiello and Olivier 2013b)

[c] Micropore volume calculated by the Dubinin-Radushkevich method.

[d] Average micropore size evaluated by the Stoeckli-Ballerini equation.

Table 3. Selected chemical paramters of the studied nanoporous carbons: Elemental analysis (wt.%) on dry ash free basis, point of zero charge, and amount of CO and CO_2 evolved from the materials upon TPD-MS.

Activated Carbon	C (wt.%)	H (wt.%)	O (wt.%)	pH_{PZC}	CO (mmol/g)	CO_2 (mmol/g)
F	96.40	0.70	2.90	8.7	698	335
F12	96.12	0.45	3.43	8.5	517	238
F24	95.96	0.39	3.65	8.8	549	205
F40	96.04	0.22	3.74	9.2	589	158

Table 4. Parameter values of the Radke-Prausnitz adsorption isotherms for adsorption of DCF from aqueous solution on the activated carbons. T = 25 °C.

Activated Carbon	pH	Q_{1200} (mg/g)	a (L/g)	b (L^{β} $mg^{-\beta}$)	β	%D
F	7	244	1.4	0.1	0.54	8.82
	WWTP	129	0.5	0.001	1.08	8.86
F12	7	524	93.4	0.6	0.84	2.26
F24	7	696	768.7	3.4	0.84	8.13
F40	7	940	836.7	2.71	0.84	9.34
	9	686	371.4	0.8	0.95	3.90
	11	528	625.7	2.3	0.91	3.96
	WWTP	679	103.5	0.31	0.90	0.18

* WWTP = Water sample from a WasteWater Treatment Plant.

Table 5. Maximum adsorption capacities of carbon materials towards DCF from aqueous solutions.

Adsorbent	Maximum adsorption capacity (mg/g)	Adsorption capacity per surface area (mg/m^2)	S_{BET} (m^2/g)	Experimental conditions	Reference
F40	1033	0.574	1801	pH = 7 T = 25 °C	This work
F24	821	0.642	1279		
F12	522	0.455	1146		
F	271	0.339	799		
Porous Carbon (Metal azolate framework-6)	503	0.161	3123	pH = 6.5	(An et al. 2018)
Graphene oxide (GO)	500	--	NA*	pH = 7 T = 20 °C	(Nam et al. 2015)
Activated biochar (pine chip)	373	0.274	1360	pH = 7 T = 25 ºC	(Jung et al. 2015)
Granular AC (F-400)	347	0.378	919	pH = 6 T = 25 ºC	(Moral - Rodríguez 2014)
Expanded graphite	330	--	NA*	No specified	(Vedenyapina et al. 2013)
Activated carbon (pine sawdust)	263.7	0.331	796	pH = 6.3 T = 30 ºC	(Álvarez-Torrellas et al. 2016)
Granular AC (F-400)	234	0.235	997	pH = 6.3 T = 23 ºC	(Sotelo et al. 2014)
Carbon xerogel treated with sulfuric acid	80.0	0.278	288	pH = 6.1 T = 30 ºC	(Álvarez et al. 2015)
AC (cocoa shell)	63.47	0.103	619	pH = 7 T = 25 ºC	(Saucier et al. 2015)
AC (Tea wate)	62	0.072	865	T ≈ 30 °C	(Malhotra et al. 2018)
Granular AC	36.23	0.078	462.96	pH = 5.5 T = 25 °C	(De Franco et al. 2018)
$CNTs/Al_2O_3$	29	0.122	237	pH = 6	(Wei et al. 2013)
AC (Cyclamen persicum tubers)	22	0.036	606.78	pH = 2 T = 25 ºC	(Jodeh et al. 2015)

* NA = No available.

Table 6. Concentrations and removal percentages of DCF, TC and TOC before and after contacting the WWTP solution containing DCF with the F40 carbon.

Sample	DCF (mg/L)	TC (mg/L)	TOC (mg/L)
WWTP without spiking DCF	0	31.9	2.41
WWTP spiked with DCF	674	289	267
WWTP spiked with DCF after adsorption on F40	150	58.5	31.8
Removal Percentage (%)	78	80	88

List of Figure Captions

Fig. 1. Adsorption-desorption isotherms of N_2 on the nanoporous carbons at 77 K (a), and pore size distributions calculated using 2D-NLDFT-HS method (b).

Fig. 2. Adsorption isotherms of CO2 at 273 K on the nanoporous carbons.

Fig. 3. Adsorption isotherms of DCF on the F carbon series at T = 25 ºC and pH = 7. The symbols represent the experimental data and the lines depict the prediction of the Radke-Prausnitz isotherm.

Fig. 4. Effect of selected textural properties on the adsorption capacities of ACs towards DCF. a) Q_{1200} vs. S_{BET}, b) U_{Norm} vs. V_P, c) U_{Norm} vs. V_{micro}, d) U_{Norm} vs. L_0.

Fig. 5. Effect of solution pH on the adsorption isotherm of DCF on F40 at T = 25 °C. The symbols represent the experimental data and the lines depict the prediction of the Radke-Prausnitz isotherm.

Fig. 6. Speciation diagram of DCF in aqueous solution as a function of the solution pH.

Fig. 7. Effect of water matrix on the adsorption of DCF on F and F40 carbons at T = 25 °C. The symbols represent the experimental data and the lines depict the prediction of the Radke-Prausnitz isotherm.

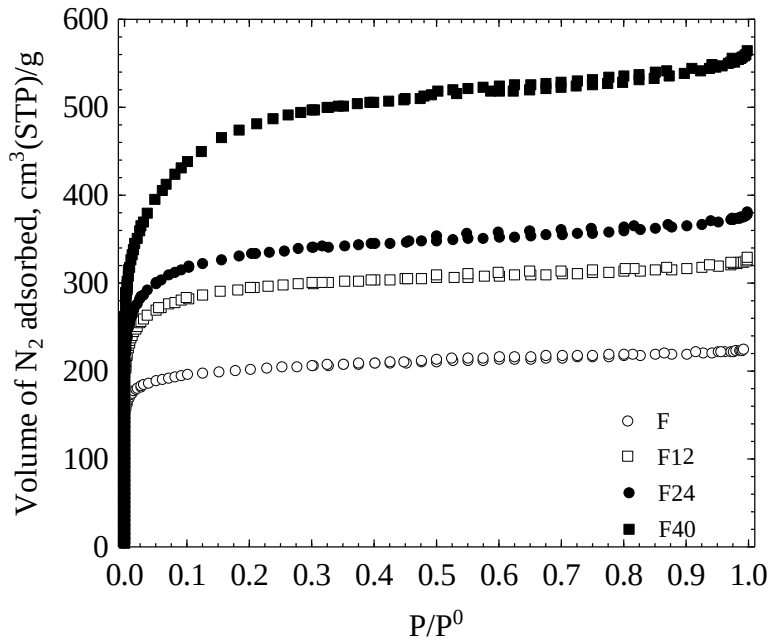
Volume of N_2 adsorbed, cm^3(STP)/g
600
500
400
300
200
100
0
0.0 0.1 0.2 0.3 0.4 0.5 0.6 0.7 0.8 0.9 1.0
P/P^0
F
F12
F24
F40

(a)

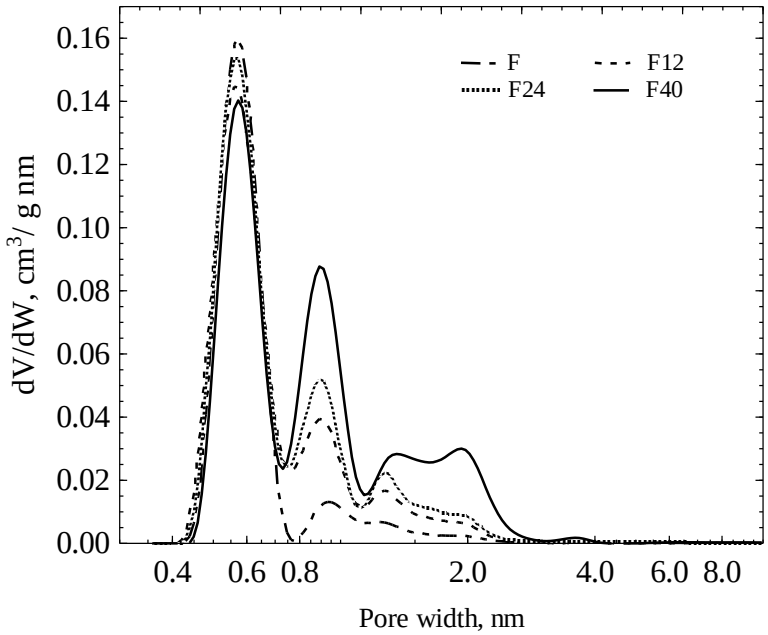
dV/dW, cm^3/ g nm
0.16
0.14
0.12
0.10
0.08
0.06
0.04
0.02
0.00
0.4 0.6 0.8 2.0 4.0 6.0 8.0
Pore width, nm
F
F12
F24
F40

(b)

Fig. 1

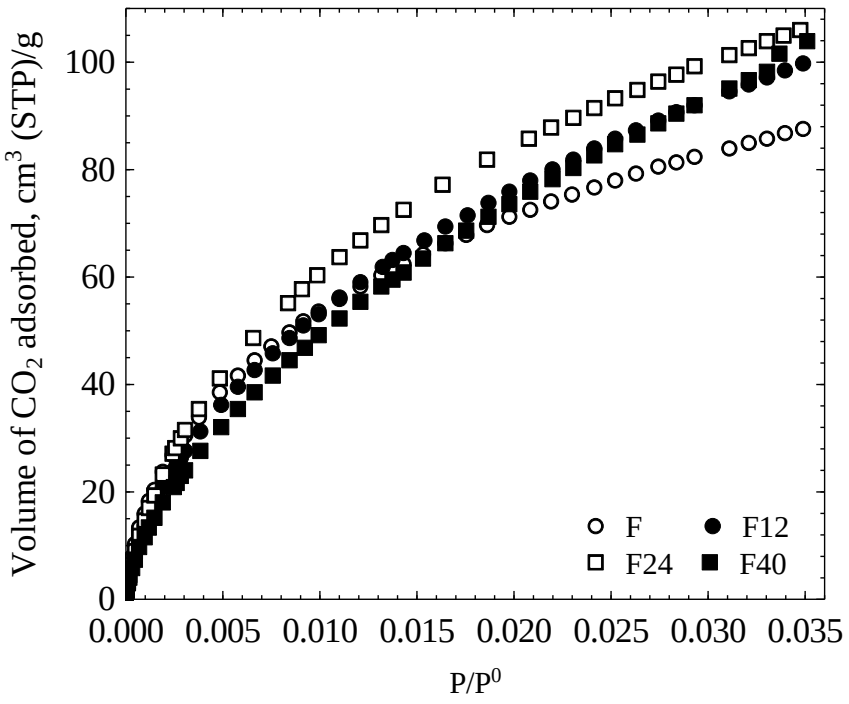
Volume of CO_2 adsorbed, cm^3 (STP)/g
0
20
40
60
80
100
0.000
0.005
0.010
0.015
0.020
0.025
0.030
0.035
P/P^0
F
F12
F24
F40

Fig. 2

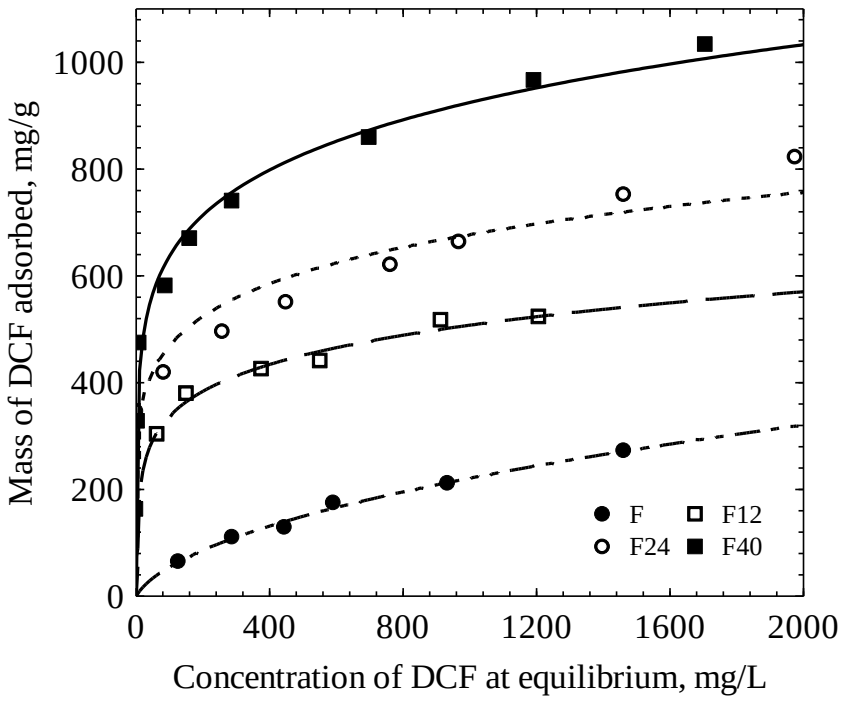
Mass of DCF adsorbed, mg/g
1000
800
600
400
200
0
0
400
800
1200
1600
2000
Concentration of DCF at equilibrium, mg/L
F
F12
F24
F40

Fig. 3

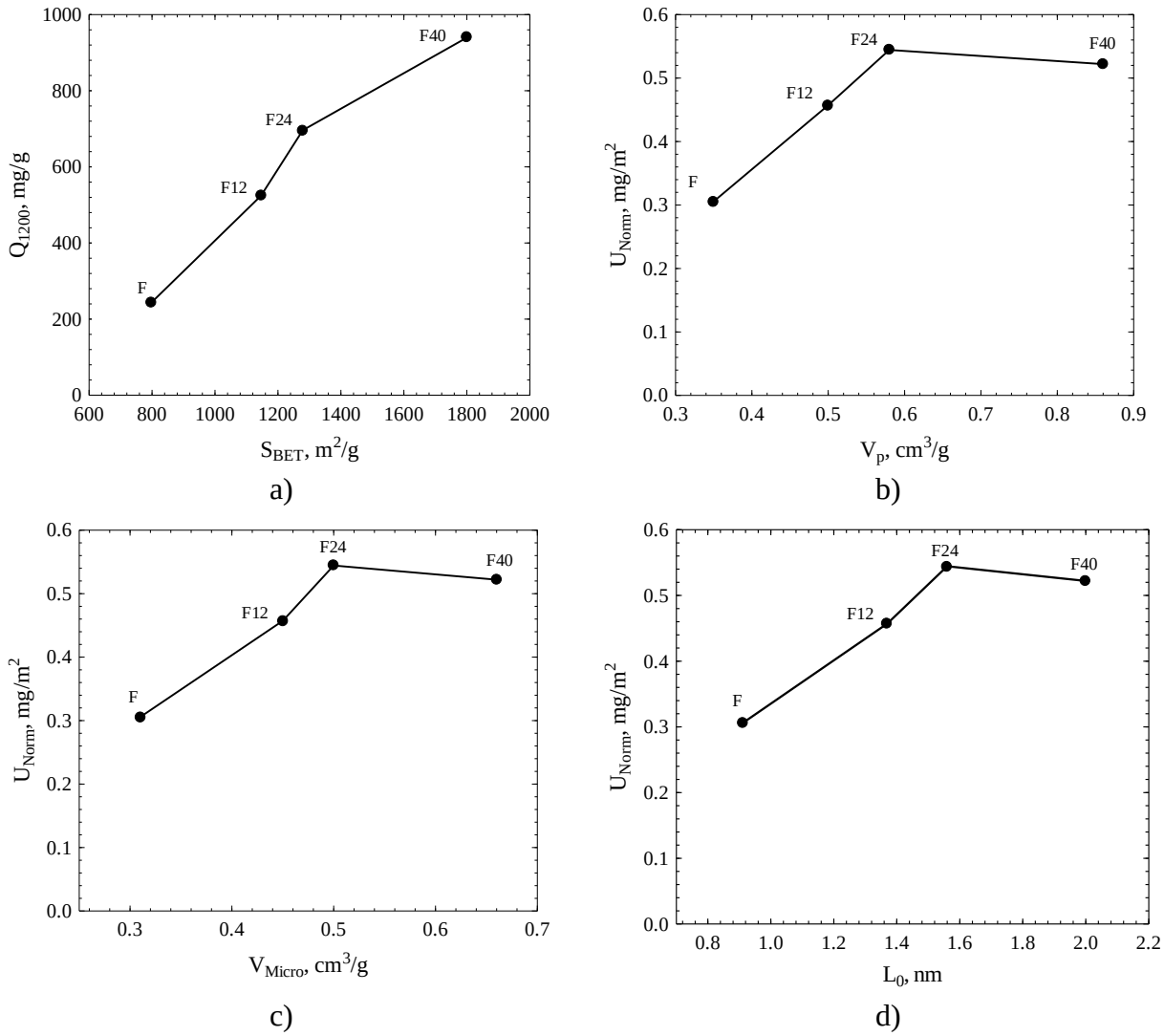
Q1200, mg/g
SBET, m2/g
F
F12
F24
F40
a)
UNorm, mg/m2
Vp, cm3/g
b)
VMicro, cm3/g
c)
L0, nm
d)

Fig. 4

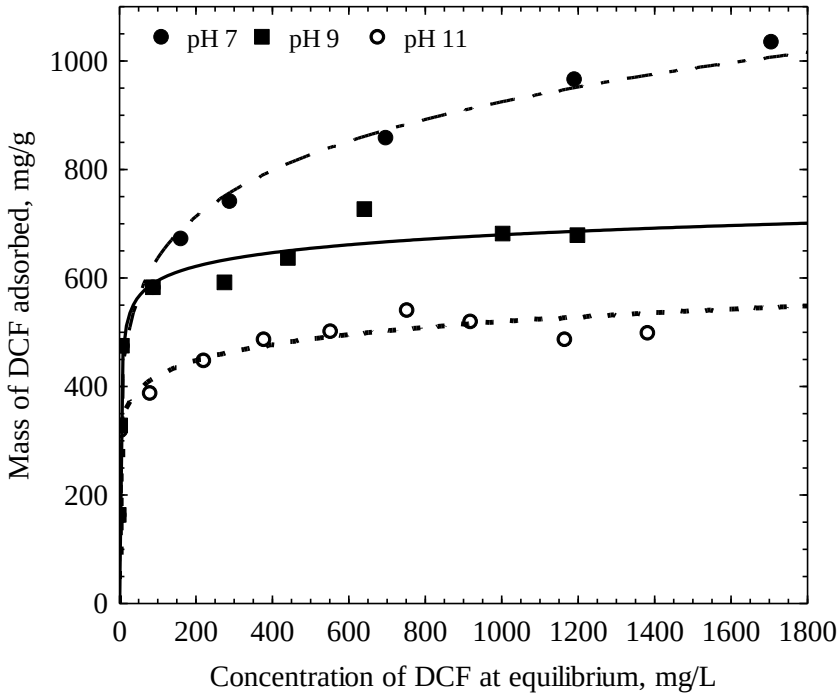
pH 7
pH 9
pH 11
Mass of DCF adsorbed, mg/g
Concentration of DCF at equilibrium, mg/L
0
200
400
600
800
1000
1200
1400
1600
1800

Fig. 5

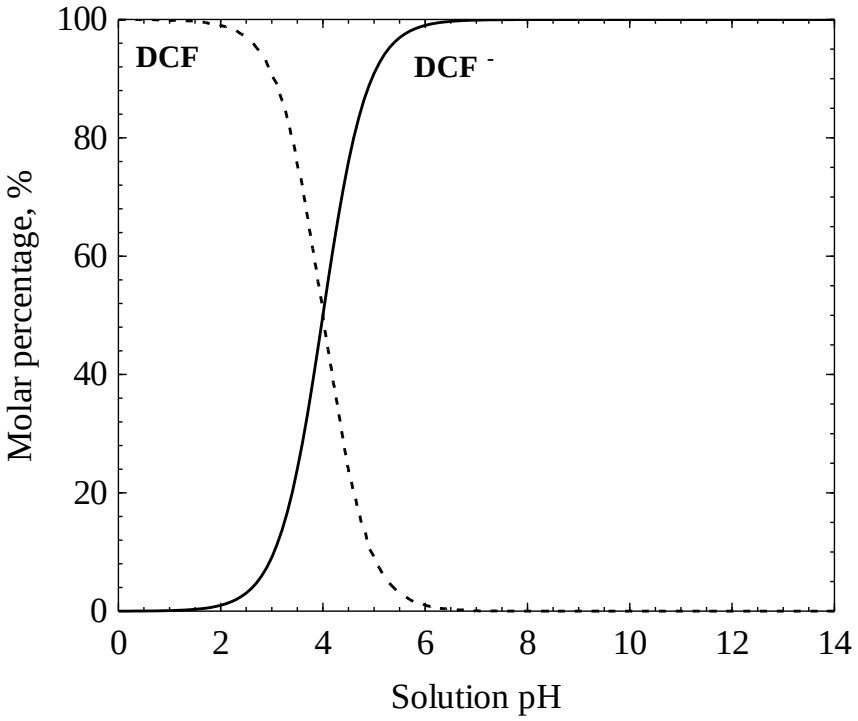
100
80
60
40
20
0
0
2
4
6
8
10
12
14
DCF
DCF -
Molar percentage, %
Solution pH

Fig. 6

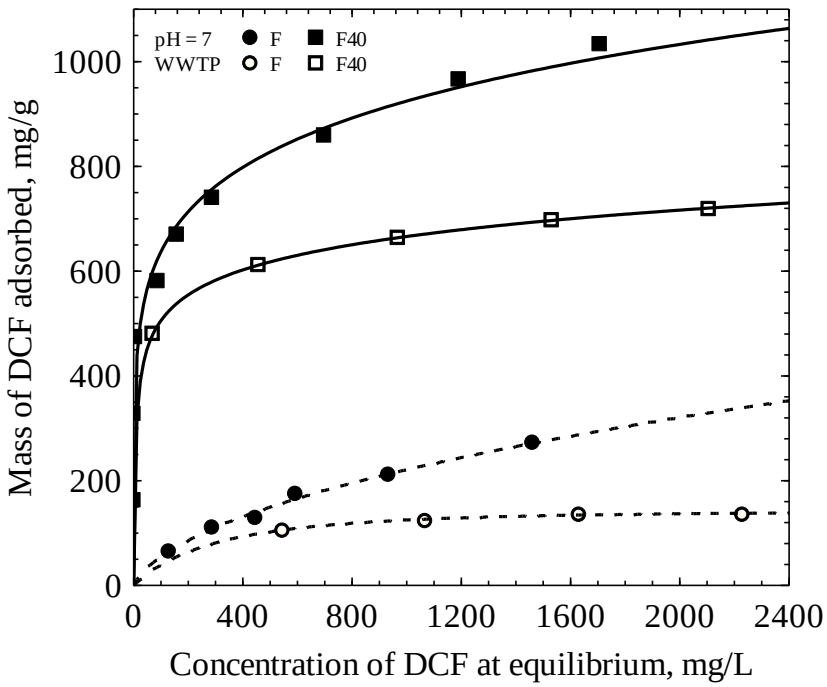
pH = 7
WWTP
F
F40
F
F40
Mass of DCF adsorbed, mg/g
Concentration of DCF at equilibrium, mg/L
0
200
400
600
800
1000
0
400
800
1200
1600
2000
2400

Fig. 7